# Penetrating power of resonant electromagnetic induction imaging

Roberta Guilizzoni, Joseph C. Watson, Paul Bartlett, and Ferruccio Renzoni

Citation: AIP Advances **6**, 095017 (2016); doi: 10.1063/1.4963299
View online: http://dx.doi.org/10.1063/1.4963299
View Table of Contents: http://scitation.aip.org/content/aip/journal/adva/6/9?ver=pdfcov
Published by the AIP Publishing

# Penetrating power of resonant electromagnetic induction imaging

Roberta Guilizzoni,[1] Joseph C. Watson,[2] Paul Bartlett,[1]
and Ferruccio Renzoni[1]
[1]*Department of Physics and Astronomy, University College London, Gower Street, London WC1E 6BT, United Kingdom*
[2]*Novel Detection Concepts, National Nuclear Security Programme, Atomic Weapons Establishment, Aldermaston, Reading RG7 4PR, United Kingdom*

(Received 6 July 2016; accepted 9 September 2016; published online 19 September 2016)

The possibility of revealing the presence and identifying the nature of conductive targets is of central interest in many fields, including security, medicine, industry, archaeology and geophysics. In many applications, these targets are shielded by external materials and thus cannot be directly accessed. Hence, interrogation techniques are required that allow penetration through the shielding materials, in order for the target to be identified. Electromagnetic interrogation techniques represent a powerful solution to this challenge, as they enable penetration through conductive shields. In this work, we demonstrate the power of resonant electromagnetic induction imaging to penetrate through metallic shields (1.5-mm-thick) and image targets (having conductivities $\sigma$ ranging from 0.54 to 59.77 $MSm^{-1}$) concealed behind them.  [http://dx.doi.org/10.1063/1.4963299]

## INTRODUCTION

Detecting objects that are concealed behind metallic screens is a central problem in many fields. These include security, where the threat represented by illicit trafficking of materials, and in particular special nuclear materials (SNM), requires reliable techniques to be developed for hazard prevention.[1,2] In many scenarios, and typically in the case of maritime cargos, a hidden target is shielded by some other material, often of unknown nature, and therefore cannot be directly identified. Techniques are thus required that allow penetration through materials, in order for the hidden target to be detected.

Recently developed electromagnetic-induction based detection techniques represent an effective solution to this challenge, since magnetic fields of appropriately low frequency can in principle penetrate through any conductive material, thus reaching the target of interest and allowing its revelation. Among these techniques, Magnetic Induction Tomography (MIT) has been exploited for producing conductivity maps of the passive electromagnetic properties of an object.[3–10] In the context of nuclear security applications, Darrer *et al.*[1,2] demonstrated an MIT-based imaging method that allows imaging of metals concealed inside ferromagnetic enclosures. Penetrating imaging, i.e. imaging of targets hidden behind a shielding material, is not only essential in the field of security. It is also a fundamental requirement in biomedicine, where diagnosis maps of the organs of interest cannot be produced without penetrating through the layers of biological tissues surrounding them. In this context, an MIT-based optical method based on the use of atomic magnetometers for diagnostic mapping of the heart's conductivity has been recently proposed by Marmugi *et al.* and Deans *et al.*[11,12]

Here we propose an alternative approach, based on resonant electromagnetic induction interrogation. We demonstrate that this method enables 2D imaging of metallic samples over a wide range of conductivities (from 0.54 to 59.77 $MSm^{-1}$),[13] even when these are concealed behind metallic shields.

 

## METHODS

This electromagnetic induction interrogation technique is based on a resonant LCR system, as shown in Fig. 1, where the inductor is the sensor. Coupling the inductor with a conductive object leads to changes in the resonant circuit parameters, such as its resonant frequency or quality factor (Q-factor), which can be detected. Operating the system at its resonant frequency

$$f_r = \frac{1}{2\pi\sqrt{LC}} \tag{1}$$

where $L$ and $C$ are the inductance and capacitance of the circuit, is known to enhance the sensitivity of detection.[14] The frequency at which the system resonates at can be varied by adjusting the circuit capacitance. In the present work, the ability to adjust the system resonant frequency has been exploited so to be able to image through conductive shields. The penetrating power of electromagnetic imaging through a shield of a given material is limited by the skin depth $\delta$:[15]

$$\delta = \sqrt{\frac{2\rho}{\omega\mu_r\mu_0}} \tag{2}$$

through which the oscillating magnetic field can penetrate through the material. Here, $\rho$ and $\mu_r$ represent the material resistivity and relative permeability, and $\omega$ the angular frequency of the oscillating magnetic field. At resonance, the frequency of the oscillating magnetic field coincides with the resonant frequency of the LCR circuit, which can be tuned by varying the capacitance.

In order to achieve a penetration through the shield, sufficient for the oscillating magnetic field to reach the target object to be imaged, the value of the capacitance is chosen so that the skin depth is either larger or of the same order of magnitude of the thickness of the shield. Therefore, by selecting an appropriate value of capacitance, the system will allow penetration through a conductive target, even when this is hidden behind shielding conductive material.

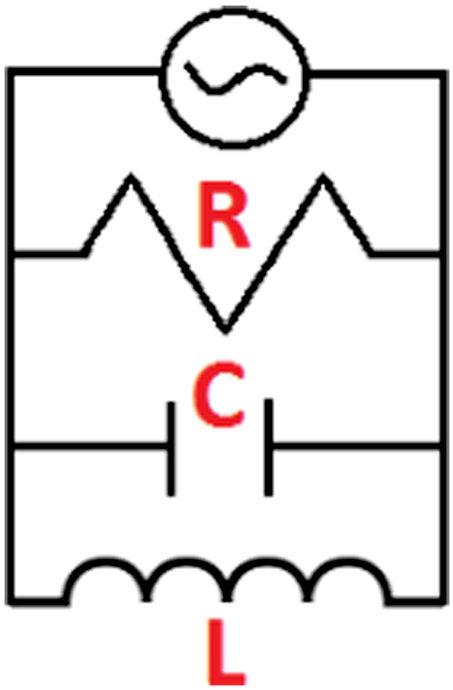


FIG. 1. Electronic schematic of the resonant electromagnetic induction system used in this work. The system capacitance can be adjusted, thus enabling penetration through the metallic shield covering the metallic target, and therefore facilitate target identification. The resistor value was R = 1KΩ ± 1%, and the inductor was a ferrite-cored coil (7.8 mm × 9.5 mm, L = 680 μH ± 10% at 1 KHz).

## RESULTS AND DISCUSSION

### 2D imaging of unshielded conductive targets

The imaging capabilities of our instruments were first investigated for unshielded targets. The magnetic coupling of a target object with the inductor leads to a change of the circuit characteristics, and in particular of the system's resonant frequency and Q-factor. These were the properties we monitored in our experiments. We have demonstrated that an image representing the target can be generated by performing position-resolved-measurements of the resonant frequency and the Q-factor, obtained by displacing the object with respect to the inductor using a computer-controlled XY stage. For each position, the system resonant frequency and the Q-factor were measured with an impedance analyser.

Typical results of our measurements, under the form of 2D plots, are shown in Fig. 2 for a conductive, non-magnetic sample of large conductivity (copper, $\sigma = 59.77$ MSm$^{-1}$), and in Fig. 3 for a lower conductivity sample, made of manganese ($\sigma = 0.54$ MSm$^{-1}$).[13] The data points in these figures represent the positions where the measurements were taken. Qualitatively, the images obtained show the system's ability to reproduce shapes by means of both resonant-frequency and Q-factor measurements.

We observed that images of higher-conductivity metals show more accurate reproduction of the samples' shapes and sizes. The copper sample's edges are more well-defined and its dimensions are closer to the ones of the actual sample, compared to the more distorted manganese images. This is caused by the larger change in the measured quantities (i.e. resonant frequency and Q-factor) that is produced by highly conductive metals, due to the larger magnitude of eddy currents induced inside them. Images similar to the ones shown in Fig. 2 were obtained for different values of skin depth, showing no dependence of the measured parameters on eddy current penetration depth. On the other hand, the manganese images obtained with resonant frequency measurements at different values of skin depths look different (see Figs. 3b and 3d); in particular, the sample's size is smaller in the image obtained with the lower skin depth. This shows a dependence of the resonant frequency shift, due to the presence of this metal, on the eddy current penetration depth. This is due to the small amount of eddy currents produced inside this metallic target, which makes it more difficult to reveal its shape and size, despite the large values of skin depth compared to the target's thickness.

A more quantitative analysis of the faithfulness of the images produced was also conducted by considering a set of aluminium disks of different diameters. For each disk, images were taken both via Q-factor and resonant frequency measurements. From these images, the contour of the disk was obtained using a Canny-edge-detection technique,[16] and a disk diameter estimated. This was

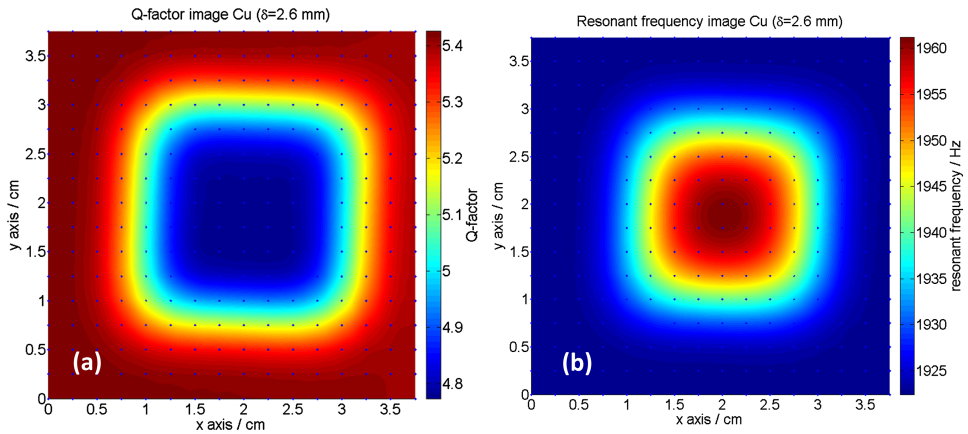


FIG. 2. Images of a copper sample ($25 \times 25 \times 1$ mm$^3$) obtained by means of position-resolved-measurements of the Q-factor (a) and the resonant frequency (b). These images demonstrate the suitability of the proposed method for imaging of high-conductivity metals.

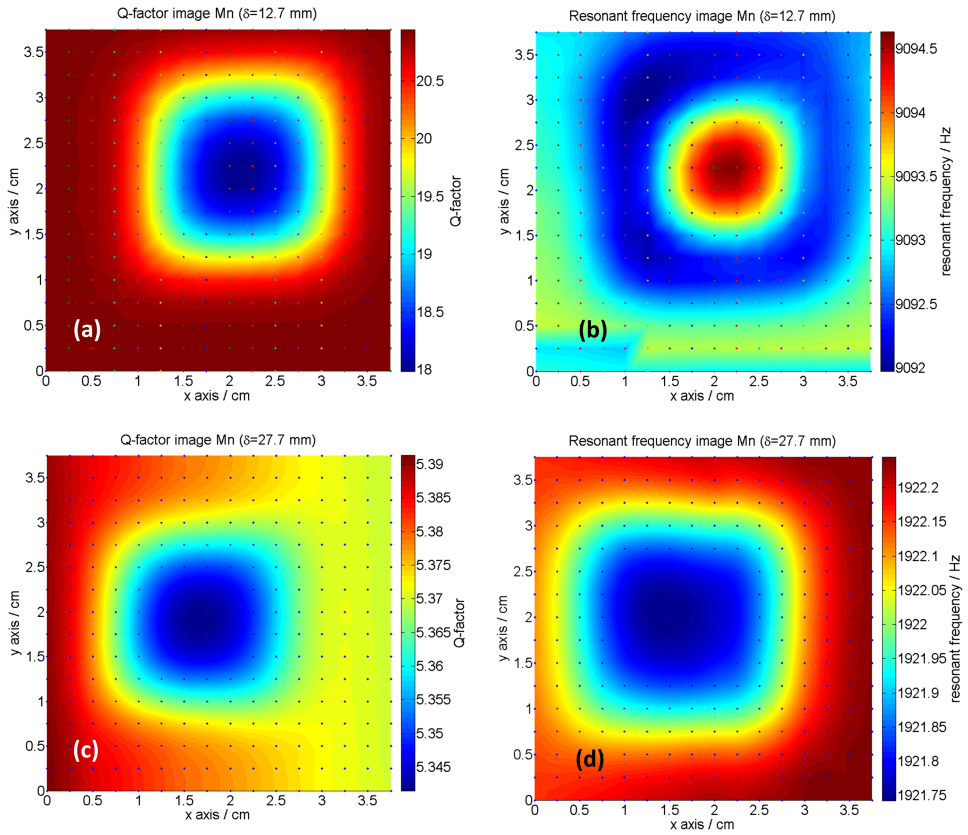


FIG. 3. Images of a manganese sample ($25 \times 25 \times 1$ mm$^3$), obtained by means of position-resolved-measurements of the Q-factor (a,c) and the resonant frequency (b,d), with the system's capacitance set to the following values: $C_1 = 0.5\,\mu$F (a,b), $C_2 = 11\,\mu$F (c,d); the corresponding skin depths were equal to $\delta_1 = 12.7$ mm and $\delta_2 = 27.7$ mm. These images prove the suitability of the proposed method for imaging of lower conductivity metals.

compared with the actual diameter (i.e. the measured diameter of the sample), with results shown in Fig. 4. The diameter estimated from the images displays a linear relationship with the samples' measured diameters, for both Q-factor and resonant frequency images, with a slope coefficient equal to unity within a few percent. This demonstrates the reliability of the imaging system for unscreened conductive target objects.

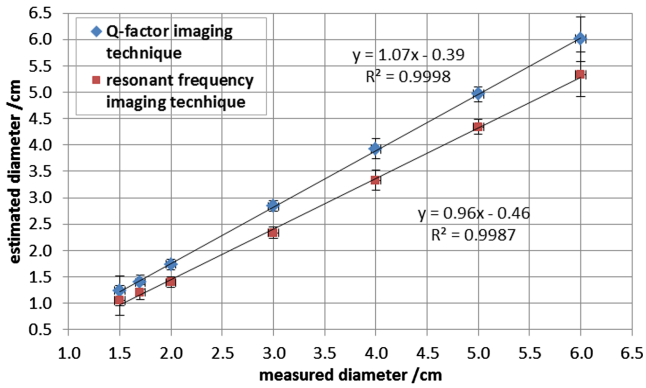


FIG. 4. Estimated diameter obtained with a Canny-edge detection method of a set of aluminium disks of different diameter (from 1.5 cm to 6 cm), plotted against diameter of the actual samples.

### 2D imaging of shielded conductive targets

Once the system capability of imaging unshielded metallic samples was assessed, the penetrating power of the imaging system was investigated. For this purpose, a sheet of highly-conductive material, i.e. a 1.5-mm-thick aluminium shield (having an area of $A = 110\times80$ mm$^2$), was introduced between the target and the sensor. The same imaging procedure adopted for 2D imaging of unshielded conductive targets was carried out, to see whether imaging of these targets in the shielded configuration was possible. Four sets of position-resolved-measurements of the resonant frequency and the Q-factor were performed, by adjusting the system capacitance to four different values, thus varying the skin depth between 0.4 mm and 2.9 mm (Table I). The selected capacitance values made the system resonate at the values reported in Table I, which were measured after placing a $25 \times 25 \times 1$ mm$^3$ copper target, covered with the aluminium shield, under the coil with lift-off equal to 0.5 cm. The images obtained with this target for each capacitance value are shown in Fig. 5.

Figs. 5a–5d show 2D surface plots obtained by means of Q-factor position-resolved-measurements, whereas Figs. 5e–5h were obtained with resonant frequency measurements. We notice that Figs. 5a and 5e do not reveal the presence of the target, due to the skin depth being too low for the magnetic field to penetrate through the aluminium shield thus not reaching the target. The skin depth was much smaller than the thickness of the shield, being equal to $\delta_1 = 0.4$ mm << 1.5 mm. The target could be revealed, using both resonant frequency and Q-factor position-resolved-measurements, for a slightly larger skin depth, equal to $\delta_2 = 0.6$ mm (Figs. 5b and 5f), despite this value being still small compared to the thickness of the shield. However, a greater skin depth, equal to $\delta_3 = 1.8$ mm, was required to achieve accurate reproduction of the target shape, when resonant frequency measurements were performed (Figs. 5f and 5g), due to the lower sensitivity of the imaging technique based on resonant frequency measurements, compared to the one based on Q-factor measurements.

Results shown in Fig. 5 demonstrate imaging of high-conductivity metals hidden behind a 1.5-mm-thick aluminium shield. This demonstrates the potential for our system to penetrate through conductive shields.

Investigations around the possibility of revealing the presence of low-conductivity shielded targets were also conducted. Fig. 6 shows 2D plots representing a manganese target, obtained by adjusting the capacitance of the system to the value C = 11 μF, corresponding to a skin depth through aluminium equal to $\delta = 3.3$ mm (the resonant frequency measured at the centre of the target was $f_r$=1.921 KHz). We observed that the skin depth required to image this low-conductivity sample is higher than the one required for imaging the copper target, due to the lower magnitude of eddy currents produced by this low-conductivity metal.

Finally, a quantitative analysis of the faithfulness of the images produced was conducted, in a similar fashion to what was performed with the unshielded targets (see Fig. 4). In this case, a set of aluminium disks of different diameter, shielded by a 1.5-mm-thick aluminium shield, were imaged both via Q-factor and resonant frequency measurements, and the contours of the disks were derived using the same Canny edge technique (*estimated diameter* in Fig. 7). This was compared with the actual disk diameters (*measured diameter* in Fig. 7). The diameter estimated from the images displays a linear relationship with the samples' measured diameters, for both Q-factor and resonant frequency images, with a coefficient of determination equal to unity within a few percent. This demonstrates the reliability of the imaging system for screened conductive target objects. A comparison between the plots reported in Figs. 4 and 7 reveals a difference in the capability of reproducing the targets'

TABLE I. Capacitance values ($C$), resonant frequency values ($f_r$)- measured at the centre of the shielded copper target- and corresponding skin depths in aluminium and copper, for each of the images shown in Fig. 5.

| Figure number | $C$ | $f_r$/KHz | δ(Al)/mm | δ(Cu)/mm |
|---|---|---|---|---|
| 5a, 5e | 20 nF | 144.225 | 0.4 | 0.3 |
| 5b, 5f | 10 nF | 66.709 | 0.6 | 0.4 |
| 5c, 5g | 1 $\mu$F | 6.598 | 1.8 | 2.1 |
| 5d, 5h | 7 $\mu$F | 2.460 | 2.9 | 2.3 |

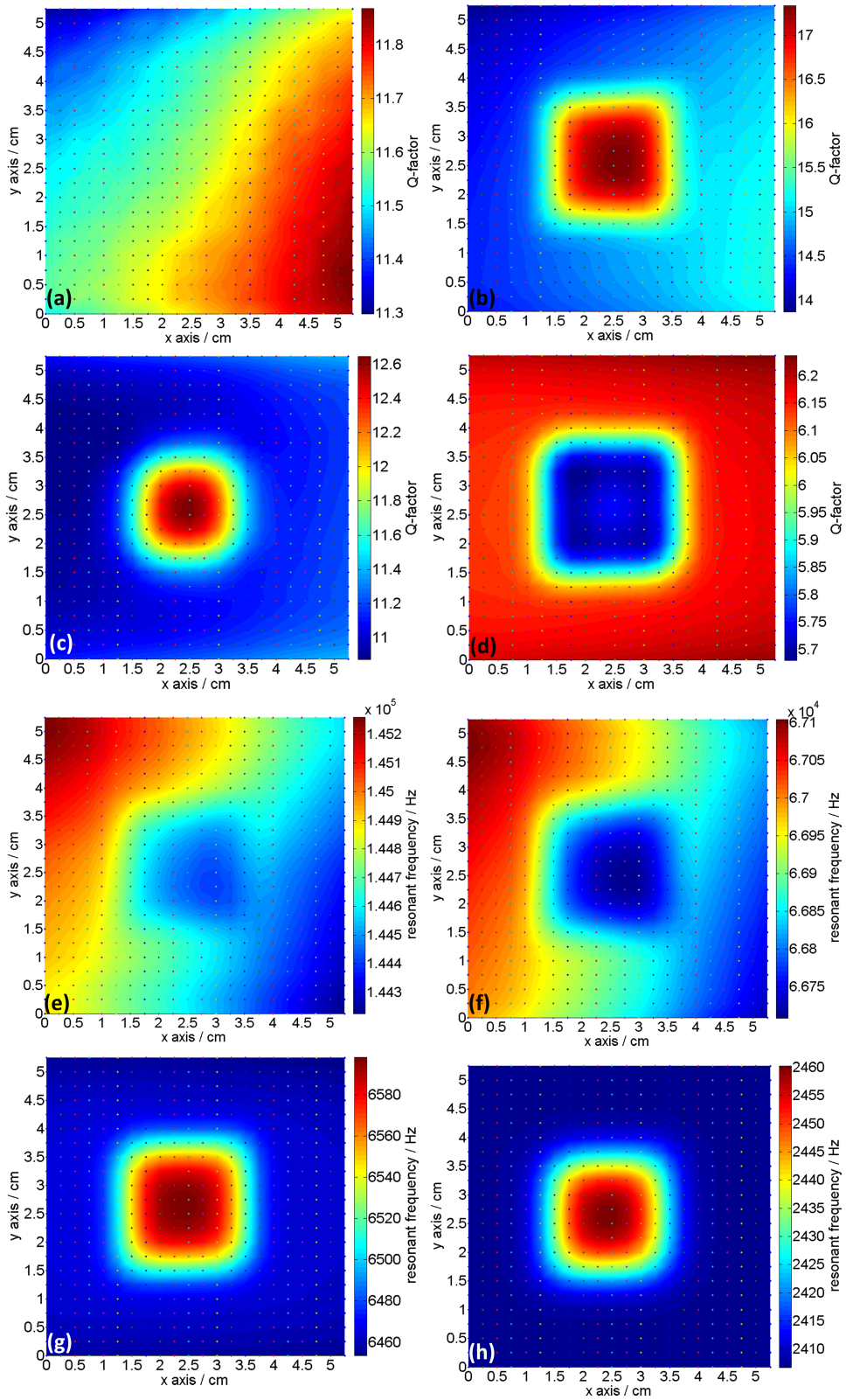


FIG. 5. Images of a copper target (25 × 25 × 1 mm$^3$) obtained by means of position-resolved-measurements of the Q-factor (a-d) and the resonant-frequency (e-h), at the following values of skin depth: $\delta_1 = 0.4$ mm (a,e), $\delta_2 = 0.6$ mm (b,f), $\delta_3 = 1.8$ mm (c,g), $\delta_4 = 2.9$ mm (d,h). During these measurements, the target was shielded by a 1.5-mm-thick aluminium sheet.

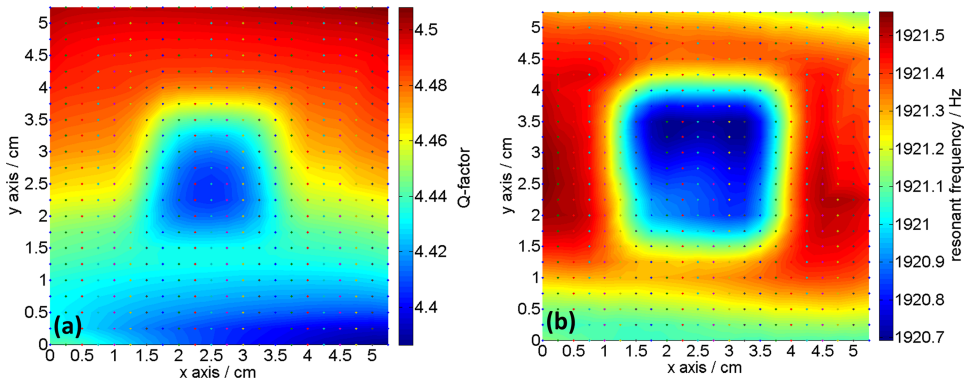


FIG. 6. Images reproducing a manganese target ($25 \times 25 \times 1$ mm$^3$), shielded by a 1.5-mm-thick aluminium sheet, obtained by means of position-resolved-measurements of the Q-factor (a) and the resonant-frequency (b), with a skin depth through aluminium equal to 3.3 mm.

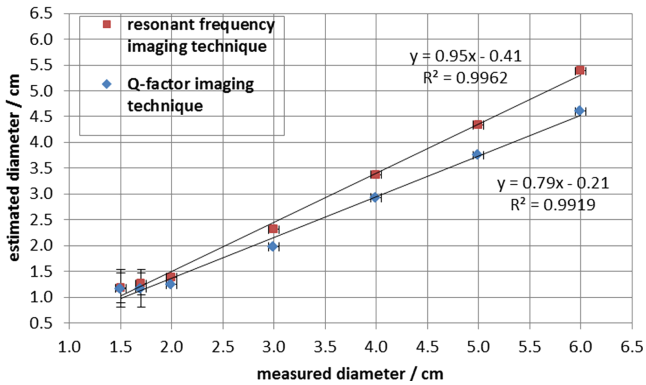


FIG. 7. Plot equivalent to the one shown in Fig. 4, obtained for aluminium disks of different diameter, shielded by a 1.5-mm-thick aluminium shield. *Estimated diameter* stands for the diameter derived by applying a Canny edge detection algorithm to the images of the disks; m*easured diameter* indicates the actual sample diameter.

dimensions of the imaging techniques based on Q-factor and resonant frequency measurements. In the case of unshielded targets, the Q-factor technique allows more accurate reproduction of the targets' dimensions than the resonant frequency technique, with an agreement within 2% between the estimated diameters and the measured ones (for disk diameters larger than 4 cm). An opposite scenario occurs with shielded targets, as images obtained with resonant frequency measurements reproduce the targets' dimensions more accurately than the Q-factor ones. Nevertheless, in both cases the diameter is underestimated (by -23% and -10% respectively, for the 6-cm diameter disk). This is due to the presence of the aluminium shield covering the targets and masking them.

The results reported in Figs. 5–7 show the suitability of our system for imaging both high and lower conductivity metals shielded by a metallic shield.

## CONCLUSIONS

The present work shows that, despite the simplicity of the system, imaging with resonant LCR circuits allows a straightforward approach to penetrate conductive shields. This can be achieved with skin depths lower than the shield thickness ($\delta = 0.6$ mm) for high conductivity targets ($\sigma = 59.77$ MSm$^{-1}$). In the case of lower conductivity targets ($\sigma = 0.54$ MSm$^{-1}$), it is sufficient to adjust the circuit components to tune the resonant frequency down to a value corresponding to a skin depth of the order of, or exceeding, the shield thickness to allow penetration ($f_r$=1.921 KHz measured at the centre of the target).

Results show that targets of both high and lower conductivity can be detected and imaged with our system. Not only can the system reveal the presence of hidden materials, it can also reproduce their shape and geometry.

The results reported here are of direct relevance to security applications, and apply in particular to scenarios involving maritime cargos.

## ACKNOWLEDGMENTS

We would like to thank Soliman Edris for writing the LabView program used in this work.

[1] B. J. Darrer, J. C. Watson, P. Bartlett, and F. Renzoni, "Magnetic imaging: A new tool for UK national nuclear security," Sci. Rep. **5**, 2271 EP (2015).
[2] B. J. Darrer, J. C. Watson, P. Bartlett, and F. Renzoni, "Electromagnetic imaging through thick metallic enclosures," AIP Adv. **5**, 087143 (2015).
[3] L. Ma, H.-Y. Wei, and M. Soleimani, "Planar magnetic induction tomography for 3D near subsurface imaging," Prog. Electromagn. Res. **138**, 65–82 (2013).
[4] M. Soleimani, "Simultaneous reconstruction of permeability and conductivity in magnetic induction tomography," J. of Electromagn. Waves and Appl. **23**, 785 (2009).
[5] S. R. Higson, P. Drake, D. W. Stamp, A. Peyton, R. Binns, A. Lyons, and W. Lionheart, "Development of a sensor for visualization of steel flow in the continuous casting nozzle," Rev. Metall./Cah. Inf. Tech. **100**, 629–632 (2003).
[6] X. Ma, A. J. Peyton, R. Binns, and S. R. Higson, "Electromagnetic techniques for imaging the cross-section distribution of molten steel flow in the continuous casting nozzle," IEEE Sensors J. **5**(2), 224–232 (2005).
[7] R. Merwa, K. Hollaus, O. Bir, and H. Scharfetter, "Detection of brain oedema using magnetic induction tomography: A feasibility study of the likely sensitivity and detectability," Physiol. Meas. **25**, 1 (2004).
[8] O. Dorn, H. Bertete-Aguirre, J. G. Berryman, and G. C. Papanicolaou, "A nonlinear inversion method for 3D electromagnetic imaging using adjoint fields," Inverse Probl **15**, 1523–1558 (1999).
[9] W. Daily and A. Ramirez, "Environmental process tomography in the United States," Chem. Eng. J. Biochem. Eng. **56**(3), 159–165 (1995).
[10] M. Noel and B. Xu, "Archaeological investigation by electrical resistance tomography: A preliminary study," Geophys. J. Int. **107**, 95–102 (1991).
[11] L. Marmugi and F. Renzoni, "Optical magnetic induction tomography of the heart," Sci. Rep. **6**, 23962 (2016).
[12] C. Deans, L. Marmugi, S. Hussain, and F. Renzoni, "Electromagnetic induction imaging with a radio-frequency atomic magnetometer," Appl. Phys. Lett. **108**, 103503 (2016).
[13] Weast, R. C. in *Handbook of Chemistry and Physics* 60th edition, Boca Raton, Florida, E85–F172 (CRC Press 1979-1980).
[14] P. Gaydecki, S. Quek, G. Miller, B. T. Fernandes, and M. A. M. Zaid, "Design and evaluation of an inductive Q-detection sensor incorporating digital signal processing for imaging of steel reinforcing bars in concrete," Meas. Sci. Technol. **13**, 1327–1335 (2002).
[15] L. Du, X. Zhu, Y. Han, L. Zhao, and J. Zhe, "Improving sensitivity of an inductive pulse sensor for detection of metal wear debris in lubricants using parallel LC resonance method," Meas. Sci. Technol. **24**(7), 1–10 (2013).
[16] J. F. Canny, "A computational approach to edge detection," IEEE Trans. Pattern Anal. Mach. Intell. **8**(6), 679–698 (1986).